



RESEARCH LETTER

10.1002/2017GL074506

Key Points:

- First empirically derived assessment of the influence of snow salinity on Arctic first-year sea ice (FYI) thickness from CryoSat-2
- Snow salinity affects FYI thickness estimates from CryoSat-2 by shifting the main radar scattering horizon upward into the snow cover
- A semi-empirically derived snow salinity correction factor is proposed for completing current methods to retrieve CryoSat-2 FYI freeboard

Supporting Information:

- Supporting Information S1

Correspondence to:

V. Nandan,
vishnunandan.nandaku@ucalgary.ca

Citation:

Nandan, V., Geldsetzer, T., Yackel, J., Mahmud, M., Scharien, R., Howell, S., ... Else, B. (2017). Effect of snow salinity on CryoSat-2 Arctic first-year sea ice freeboard measurements. *Geophysical Research Letters*, 44, 10,419–10,426. <https://doi.org/10.1002/2017GL074506>

Received 9 JUN 2017

Accepted 30 SEP 2017

Accepted article online 6 OCT 2017

Published online 17 OCT 2017

Effect of Snow Salinity on CryoSat-2 Arctic First-Year Sea Ice Freeboard Measurements

Vishnu Nandan¹ , Torsten Geldsetzer¹, John Yackel¹ , Mallik Mahmud¹ , Randall Scharien² , Stephen Howell³ , Joshua King³ , Robert Ricker^{4,5} , and Brent Else¹

¹Cryosphere Climate Research Group, Department of Geography, University of Calgary, Calgary, Alberta, Canada,

²Department of Geography, University of Victoria, Victoria, British Columbia, Canada, ³Climate Research Division,

Environment and Climate Change Canada, Toronto, Ontario, Canada, ⁴Alfred Wegener Institute, Helmholtz Centre for Polar and Marine Research, Bremerhaven, Germany, ⁵University Brest, CNRS, IRD, Ifremer, Laboratoire d'Océanographie Physique et Spatiale (LOPS), IUEM, Brest, France

Abstract The European Space Agency's CryoSat-2 satellite mission provides radar altimeter data that are used to derive estimates of sea ice thickness and volume. These data are crucial to understanding recent variability and changes in Arctic sea ice. Sea ice thickness retrievals at the CryoSat-2 frequency require accurate measurements of sea ice freeboard, assumed to be attainable when the main radar scattering horizon is at the snow/sea ice interface. Using an extensive snow thermophysical property dataset from late winter conditions in the Canadian Arctic, we examine the role of saline snow on first-year sea ice (FYI), with respect to its effect on the location of the main radar scattering horizon, its ability to decrease radar penetration depth, and its impact on FYI thickness estimates. Based on the dielectric properties of saline snow commonly found on FYI, we quantify the vertical shift in the main scattering horizon. This is found to be approximately 0.07 m. We propose a thickness-dependent snow salinity correction factor for FYI freeboard estimates. This significantly reduces CryoSat-2 FYI retrieval error. Relative error reductions of ~11% are found for an ice thickness of 0.95 m and ~25% for 0.7 m. Our method also helps to close the uncertainty gap between SMOS and CryoSat-2 thin ice thickness retrievals. Our results indicate that snow salinity should be considered for FYI freeboard estimates.

1. Introduction

Satellite radar altimetry from the European Space Agency's CryoSat-2 (CS-2) is widely used to provide estimates of Arctic sea ice thickness and mass balance (e.g., Kwok & Cunningham, 2015; Laxon et al., 2013). Under an assumption of isostatic equilibrium, sea ice thickness estimates are primarily a function of sea ice freeboard and snow load (e.g., Ricker et al., 2014). Measurement of the sea ice freeboard relies on the altimeter radar penetrating the snow cover to interact with the snow/sea ice interface. In the case of CS-2, the reflected radar signal (i.e., the main scattering horizon) is assumed to be at the snow/sea ice interface (Hendricks et al., 2016; Laxon et al., 2013). However, the snow cover on sea ice affects the CS-2 radar waves, and it is acknowledged that this may lead to a vertical shift in the location of the main scattering horizon (e.g., Ricker et al., 2015; Willatt et al., 2011). Such a shift has the potential to misrepresent the sea ice freeboard, leading to ambiguous sea ice thickness estimates (e.g., Ricker et al., 2014; Tilling et al., 2015).

Several studies discuss factors that can contribute to snow cover interactions with the CS-2 radar signal, including footprint-scale surface roughness variations (Kwok, 2014), potential dependence on snow temperature (Willatt et al., 2011), snow volume scattering-induced bias (Hendricks et al., 2016; Ricker et al., 2014, 2015), and overestimation or underestimation of the measured freeboard due to snow compression (Kern et al., 2015; Tilling et al., 2015). However, no study has investigated the impact of snow salinity on CS-2 signal penetration.

During the formation of seasonal first-year sea ice (FYI), a small amount of brine is expelled upward, resulting in a thin brine layer on the ice surface. With subsequent snow accumulation, there is an upward wicking of brine from the ice surface into the snow cover. This wicking produces brine-wetted snow, primarily within the bottom 6–8 cm, which have salinities ranging from 1 to 20 parts per thousand (Barber et al., 1995; Crocker, 1992; Geldsetzer et al., 2009). In thicker snow covers, strong salinity gradients are commonly observed in the bottommost layers, with significantly lower brine volumes, or brine-free conditions, in the uppermost snow layers (Drobot & Barber, 1998; Fuller et al., 2014). The brine within the snow alters the

Table 1

Snow Thickness and Snow Pit Metadata From Measurements Made on First-Year Sea Ice in the Canadian Arctic Archipelago

Field campaign	Month, year	# of spatially independent snow thickness measurements	# of snow pits	Reference
Cambridge Bay (69.03°N; 105.12°W)	April 2014 and 2017 and May 2016	~4,150	43	Zheng et al. (2017)
Eureka (80.08°N; 86.77°W)	April 2014, 2016	~2,550	59	King et al. (2015)
Resolute Bay (74.7°N; 95.6°W)	May 2012	~650	44	Nandan et al. (2017, 2016)
Hudson Bay (58.46°N; 93.50°W)	April 2009	~350	38	Fuller et al. (2014)
Cape Bathurst (69.63°N; 126.11°W)	May 2004 and 2008	~750	29	Barber and Hanesiak (2004)

dielectric and microwave scattering properties of the snow (Barber & Nghiem, 1999; Drinkwater & Crocker, 1988; Geldsetzer et al., 2009), leading to strong microwave attenuation within the snow volume, with significantly reduced radar penetration (e.g., Nandan et al., 2017). These factors likely also affect the location of the CS-2 main scattering horizon.

Brine-wetted snow is found predominantly on FYI (Drinkwater & Crocker, 1988; Geldsetzer et al., 2009), whereas on older, thicker multiyear sea ice (MYI), snow salinity is negligible because brine drainage occurs through the ice during repeated summer melt cycles. The upper layers of MYI ice thus are also brine-free. Therefore, MYI and FYI interact with the CS-2 radar signal in markedly different ways, with MYI allowing greater CS-2 signal penetration, while FYI inhibits the CS-2 signal. Under the influence of a warming Arctic, the proportion of FYI is increasing and that of MYI decreasing (Maslanik et al., 2011). Additionally, a warming Arctic, with increasingly thinner snow covers on FYI in many parts of the Arctic (e.g., Webster et al., 2014), and these snow covers are likely to be more saline. The influence of brine-wetted snow on FYI is thus an increasingly relevant factor affecting satellite altimeter measurements.

In this study, we propose a semiempirical approach to quantify the effect of snow salinity on CS-2-estimated FYI freeboard and thickness estimates. Using snow property measurements on FYI acquired from various locations in the Canadian Arctic during late winter season, we characterize the brine volume and dielectric property distribution in snow-covered FYI. We then model the main scattering horizon and maximum penetration depth at the CS-2 frequency (13.575 GHz). Next, we establish a snow salinity correction factor, as a function of snow thickness, to be used in the determination of sea ice freeboard from CS-2. Finally, we use the corrected freeboard to estimate FYI thickness from CS-2 and compare this with a CS-2 FYI thickness retrieval estimate from March 2016 produced by Ricker et al. (2017). A stepwise flowchart (F1) is included in the supporting information to provide additional information on the modeled parameterization of the main scattering horizon and the correction factor.

2. Data and Methods

2.1. Sea Ice Freeboard Data

Ice freeboard (F_I) from CS-2 was obtained from the Alfred Wegener Institute data products (<http://www.meer-eisportal.de>) (Grosfeld et al., 2016; Ricker et al., 2014). These data are based on a threshold-first-maximum retracker algorithm (TFMRA) that locates the main scattering horizon at 50% of the first local maximum of the radar waveform. Following subtraction of the mean sea surface and local sea surface anomalies, the radar freeboard (F_R) is assumed to be at the snow/ice interface (Hendricks et al., 2016). With regards to the snow cover, only a single correction factor (C_W) (Kwok, 2014) is applied, to account for the reduced propagation speed in the snow cover given by (1):

$$F_I = F_R + C_W \tag{1}$$

2.2. Snow and Sea Ice Data

Field data from FYI were collected during nine field campaigns in the Canadian Arctic. These campaigns took place during the late winter season (April and May) from 2004 to 2017, on both undeformed and slightly deformed FYI (Figure S1 in the supporting information and Table 1). These data encompass 53,000 snow thickness measurements and 213 detailed snow pits. To minimize spatial autocorrelation of snow thickness measurements, a lag distance threshold of 15 m is used to select only spatially independent measurements,

following the semivariogram methodology of Iacozza and Barber (1999). This reduces the number of snow thickness measurements to 8,500. The mean snow thickness (H_S) of these 8,500 measurements is 16 ± 6 cm (with a modal snow thickness of 14 cm). The 213 snow pits range in snow thickness from 4 cm to 40 cm. Snow pit thermophysical properties were sampled at 2 cm vertical resolution and include snow salinity (S_S), snow temperature (T_S), and snow density (ρ_S).

2.3. Brine Volume and Penetration Depth Modeling

Brine volume fraction φ_{bs} is estimated following Drinkwater and Crocker (1988),

$$\varphi_{bs} = \left[\frac{\varphi_{bsi}\rho_b}{(1 - \varphi_{bsi})\rho_i + \varphi_{bsi}\rho_b} \right] \left[\frac{\rho_s}{\rho_b} \right] \quad (2)$$

where ρ_i is the temperature-dependent density of pure ice in g/cm^3 , ρ_b is the density of brine in g/cm^3 as a function of temperature-dependent brine salinity (Cox & Weeks, 1975), and φ_{bsi} is the temperature-dependent brine volume fraction of sea ice (Frankenstein & Garner, 1967).

CS-2 penetration depth δ_p into the snow cover, ignoring scattering losses is derived following Ulaby et al. (1984):

$$\delta_p = \frac{\lambda_0}{4\pi} \left\{ \frac{\varepsilon'}{2} \left[\left(1 + \left(\frac{\varepsilon''}{\varepsilon'} \right)^2 \right)^{1/2} - 1 \right] \right\}^{-1/2} \quad (3)$$

where λ_0 is the wavelength (0.02 m for CS-2). ε' and ε'' represent the modeled dielectric permittivity and loss, respectively. Employing the snow density data and the estimated brine volume, we calculate ε' and ε'' for each snow layer. For fresh dry snow on FYI, ε' equals the permittivity of dry snow ε'_{ds} , which is frequency independent:

$$\varepsilon'_{ds} = 1 + 2.55\rho_{ds} \quad (4a)$$

where ρ_{ds} is the density of dry snow (Geldsetzer et al., 2009).

For snow layers that are brine-wetted, ε' becomes the permittivity of brine-wetted snow ε'_{bs} , calculated using a dielectric mixture model (Geldsetzer et al., 2009):

$$\varepsilon'_{bs} = \varepsilon'_{ds} + S\varphi_{bs}\varepsilon'_b \quad (4b)$$

where ε'_{ds} is obtained by removing the brine volume from the measured snow density, S is a saturation-dependent dielectric depolarization factor, set to 1.33 (Geldsetzer et al., 2009), and ε'_b is the temperature- and frequency-dependent permittivity of brine (Stogryn & Desargant, 1985).

For fresh dry snow layers on FYI, ε'' equals the dielectric loss of dry snow (ε''_{ds}), which is <0.01 (Denoth, 1989); ε'' is set to 0.001 in this study. For snow layers that are brine-wetted, ε'' becomes the dielectric loss of brine-wetted snow (ε''_{bs}) and is also calculated using a dielectric mixture model, as the sum of the dielectric loss of dry snow, and the conductivity and relaxation contributions owing to brine inclusions. Detailed description of the dielectric mixture model can be found in Geldsetzer et al. (2009).

The two-way loss $L(\theta')$ for a snow layer is given by (Winebrenner et al., 1992)

$$L(\theta') = \exp\left(\frac{-2K_e\tau}{\cos\theta'}\right) \quad (5)$$

where the extinction coefficient K_e is the inverse of δ_p , θ' is the incidence angle within the snow layer based on the degree of refraction, and τ is the snow layer thickness (0.02 m).

Maximum δ_p is attained using the equation $P(d)/P(0_+) = 1/e$, where $P(0_+)$ is the power at the air/snow interface and $P(d)$ is the power at depth d (Winebrenner et al., 1992). Hence, the deepest layer to which microwaves penetrate corresponds to approximately one-third of the initial power that enters the snow layer.

2.4. Modeled Scattering Horizon

The main scattering horizon (S_H) is modeled as the vertical distance from the air/snow interface. In a multi-layered system such as snow covered FYI, S_H is a function of the snow thermophysical properties through

which the CS-2 altimeter signal propagates (Ricker et al., 2014). Nevertheless, the dominant scattering mechanism for FYI is expected to be surface scattering, especially at the CS-2 incidence angle.

To obtain a first-order estimate of the dominant surface scattering interface (i.e. S_H) in snow-covered FYI, we model the Ku-band transmission, reflection (Lorrain et al., 1988), and two-way loss (Winebrenner et al., 1992) for a multilayered snow cover. The simulated normalized echo power P_T at each n^{th} snow layer is derived using (6a) and (6b)

$$P_{T(n \geq 2)} = (1 - P_{n-1})^* \left[\prod_{k=2}^{n-1} \left\{ T_k(\theta')^* \Pi \left(1 - \prod_{k=2}^{n-1} L_k(\theta') \right) \right\} \right]^* R_n(\theta') \quad (6a)$$

while

$$P_1 = R_1(\theta) \quad (6b)$$

where $L(\theta')$ is the two-way loss factor given the refracted incidence angle θ' . $T(\theta')$ and $R(\theta')$ are the power transmission and reflection coefficients at the upper surface of each snow layer, given the θ' in the layer immediately above it. θ in ((6b)) represents the incidence angle at which the CS-2 signal interacts with the air/snow interface. The snow layer with the maximum P_T is identified as the S_H . In radar altimetry of ice, the dominant surface scattering interface is associated with a point at 50% of the first local maximum of the waveform (Davis, 1997). Therefore, S_H corresponds to the 50% TFMRA used by Ricker et al. (2014, 2017) and Hendricks et al. (2016).

2.5. Snow Salinity Correction Factor

The portion of a FYI snow cover lying below S_H is the estimated vertical shift in the scattering horizon due to snow salinity. We term this the snow salinity correction factor (Δ_S). Building on equation (1), we propose a snow salinity correction factor Δ_S that can be applied to CS-2 estimated F_I for FYI, thus

$$F_I = F_R + C_W + \Delta_S \quad (7)$$

Other snow cover correction factors have been proposed (e.g., Hendricks et al., 2016; Kern et al., 2015; Kwok, 2014; Ricker et al., 2014, 2015; Tilling et al., 2015; Willatt et al., 2011); however, these are not applied to the freeboard product used in this study. Possible effects of Δ_S on C_W and other correction factors are not investigated in this study and warrant further research.

2.6. Sea Ice Thickness

Sea ice thickness (T) is derived assuming isostatic equilibrium using

$$T = F_I \frac{\rho_W}{\rho_W - \rho_I} + H_S \frac{\rho_S}{\rho_W - \rho_I} \quad (8)$$

where ρ_W is the density of seawater (1,024 kg/m³), ρ_I is the density of sea ice density (916.7 kg/m³ for FYI), H_S is the snow thickness, and ρ_S is the density of snow.

This equation is used to estimate T from the measured F_I , using assumed snow properties (e.g., Kwok & Cunningham, 2015; Laxon et al., 2013; Ricker et al., 2014). The H_S for MYI is generally obtained from the Warren snow climatology (Warren et al., 1999), whereas the H_S for FYI is most often assumed to be 50% of the Warren snow climatology (Kurtz & Farrell, 2011). ρ_S is also obtained from the Warren snow climatology. FYI is distinguished from MYI using the daily Ocean and Sea Ice Satellite Application Facility ice concentration product (Eastwood, 2012).

We apply the snow salinity correction factor (i.e. $\Delta_S = H_S - S_H$) via equation (7) (F_I) in conjunction with equation (8), to estimate FYI ice thickness (T_{FYI}) for the entire Arctic. We compare this snow salinity-corrected retrieval with the standard FYI thickness retrieval from March 2016 produced by Ricker et al. (2017). CS-2 retrievals are likely not appropriate for thin FYI (i.e., $< \sim 0.5$ m) (Ricker et al., 2017). Therefore, we also demonstrate the Soil Moisture and Ocean Salinity (SMOS) L-band radiometer data as a complementary product for thin FYI thickness retrievals (Tian-Kunze et al., 2014).

2.7. Sea Ice Thickness Error Analysis

FYI thickness retrieval error is assessed as the relative error E_R , which is defined as the ratio between the ice thickness uncertainty and the ice thickness (Hendricks et al., 2016; Ricker et al., 2017). The E_R of the original FYI

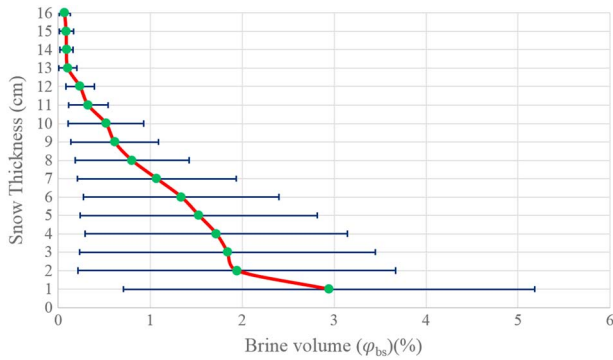


Figure 1. Mean brine volume (ϕ_{bs}) as a function of snow thickness for 16 cm snow covers on FYI. The error bars $\phi_{bs(-1\sigma)}$ and $\phi_{bs(+1\sigma)}$ represent one standard deviation ($\pm 1\sigma$) from the mean ϕ_{bs} . The snow/sea ice interface is located at 0 cm on the y axis.

thickness retrieval (Ricker et al., 2017) (hereafter $T_{FYI(ORIG)}$) is compared with the E_R of the snow salinity-corrected T_{FYI} using Δ_S (hereafter $T_{FYI(\Delta_S)}$). E_R follows a positively skewed, non-normal distribution (Ricker et al., 2017); therefore, we employ running medians (based on 20 cm wide bins) to illustrate trends. This is in contrast to the running means used by Ricker et al. (2017) and Kaleschke et al. (2015), which overestimate E_R due to the skewedness.

3. Results and Discussion

3.1. Empirical Distribution of Brine Volume in Snow-Covered FYI

The brine volume distribution in the snow-covered FYI in our dataset ranges from 0% (brine-free) to ~6%. The highest brine volumes are found at the snow/sea ice interface, decreasing with height into the snow cover. These observations are consistent with the upward brine wicking mechanism expected to occur within the bottom 6–8 cm of the snow cover over-

laying FYI (Barber et al., 1995; Crocker, 1992; Drinkwater & Crocker, 1988; Geldsetzer et al., 2009; Nandan et al., 2017). For snow thicknesses ≤ 8 cm, the snow is usually found to be completely brine-wetted. For snow thicknesses > 8 cm, the brine volume gradient culminates in very low brine volume in the uppermost layers.

As an example of the brine volume ϕ_{bs} distribution in snow-covered FYI, we illustrate snow pit data ($n = 36$) for a snow thickness of 16 cm (Figure 1). This case study corresponds to the mean snow thickness observed in our dataset. Nearly brine-free snow ($\phi_{bs} < 0.1\%$) is observed in the top 4 cm, below which ϕ_{bs} increases to ~1% at 7 cm above the ice surface and increases further to ~2% at 2 cm above the ice surface.

The ϕ_{bs} distribution at minus one standard deviation ($\phi_{bs(-1\sigma)}$) represents less saline and moderately cold snow covers within the dataset (Figure S2c). In such cases, the snow cover is brine-free for the top 4 cm, below which it has low brine volumes ($< 0.2\%$), with somewhat higher brine volume found only immediately above the snow/sea ice interface. The ϕ_{bs} distribution at plus one standard deviation ($\phi_{bs(+1\sigma)}$) represents relatively warmer, more-saline snow covers within the dataset (Figure 1). In such cases, the snow cover can reach ~1% ϕ_{bs} at 10 cm, ~2% ϕ_{bs} at 7 cm, and $> 5\%$ ϕ_{bs} at 1 cm; however, the top 4 cm still have relatively low brine volume.

It is important to note that the brine volume distributions in our dataset were obtained during late winter conditions on thick FYI. During the early winter, shortly after sea ice formation, the brine volume distribution may exhibit even higher values, due in part to thinner snow covers and warmer air and ice temperatures (e.g., Drinkwater & Crocker, 1988). Conversely, in midwinter, snow covers likely exhibit reduced brine volumes, as snow temperatures are at a minimum. Given the large snow temperature range of our dataset (Figure S2b), the brine volume variance in our dataset is expected to reasonably represent the majority of spatiotemporal variance in the Canadian Arctic.

3.2. CryoSat-2 Scattering Horizon, Penetration Depth, and Snow Salinity Correction Factor

Based on the brine volume distributions, Δ_S is calculated for snow thicknesses from 4 to 40 cm, via equations (4a) through (7) (Figure 2). A cubic fit provides a first estimate of the trend of Δ_S as a function of snow thickness H_S :

$$\Delta_S = 1.4022229 + 0.9114689H_S - 0.0437265H_S^2 + 0.00061H_S^3 \quad (9)$$

Although data are somewhat scarce for some snow thicknesses, there are some notable trends. For $H_S \leq 8$ cm, Δ_S is within 2 cm of the snow surface, the result of shallow snow usually being brine-wetted throughout. For $10 \text{ cm} \leq H_S \leq 24$ cm, $\Delta_S \approx 7$ cm, and for $H_S \geq 26$ cm, $\Delta_S \approx 6$ cm. The consistency of Δ_S for snow thicknesses ≥ 10 cm is supported by observations of

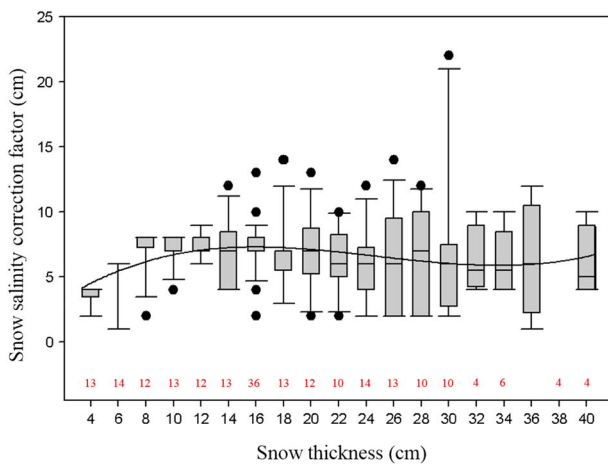


Figure 2. Box and whisker plot illustrating the statistical relationship of the snow salinity correction factor (Δ_S), as a function of snow thickness (H_S) for the snow thickness range of the snow pit data set. The numbers highlighted in red represent the number of snow pits under each snow thickness.

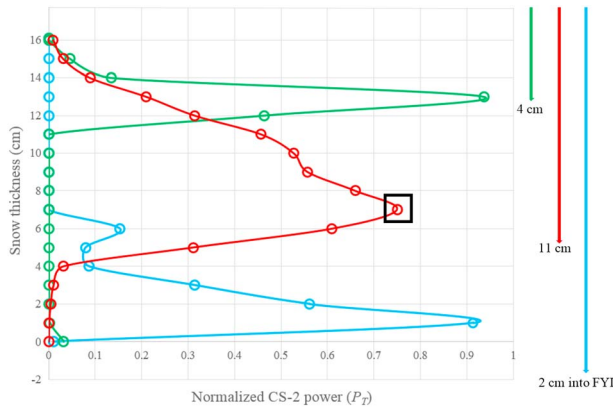


Figure 3. Simulated normalized echo power for 16 cm snow covers on FYI. The green, red, and blue lines represent power values for the distributions of $\varphi_{bs(+1\sigma)}$, φ_{bs} , and $\varphi_{bs(-1\sigma)}$, respectively. The downward green, red, and blue arrows indicate the maximum penetration depth for $\varphi_{bs(+1\sigma)}$, φ_{bs} , and $\varphi_{bs(-1\sigma)}$, respectively. The black square represents the S_H for φ_{bs} . The snow/sea ice interface is located at 0 cm on the y axis.

brine-wetted snow typically being confined within the bottom 6–8 cm of the snow cover overlaying FYI (Barber et al., 1995; Drinkwater & Crocker, 1988; Geldsetzer et al., 2009; Nandan et al., 2017). Therefore, a consistent value of $\Delta_S = 7$ cm could reasonably be used for snow thicknesses >8 cm.

The standard error (SE) of the regression is 2.7 cm, providing an indication of the spatiotemporal variability in Δ_S that may be encountered in the Canadian Arctic. To illustrate the effects of this variability on FYI thickness retrievals, we used the 16 cm snow pit case study data to calculate the position of Δ_S corresponding to φ_{bs} , as well as the scattering horizons corresponding to $\varphi_{bs(-1\sigma)}$ and $\varphi_{bs(+1\sigma)}$; these are $\Delta_{S(-1SE)}$ and $\Delta_{S(+1SE)}$, respectively (Figure 3).

For a 16 cm snow cover with mean φ_{bs} distribution, the maximum power S_H occurs 9 cm below the air/snow interface, and Δ_S is thus 7 cm above the snow/ice interface (equation (6a)) (red line and black square in Figure 3). The simulated CS-2 radar signal has a maximum penetration (δ_p) of 11 cm into the snowpack (downward red arrow in Figure 3), where the high salinity and associated dielectric loss ($\epsilon'' > \sim 0.32$) in the bottom snow layers lead to signal absorption.

In the case of cold, nearly brine-free conditions (i.e. $\varphi_{bs(-1\sigma)}$), the $S_{H(-1\sigma)}$ is 15 cm below the air/snow interface, and thus, $\Delta_{S(-1SE)}$ is only 1 cm above the snow/sea ice interface (Figure 3). The CS-2 radar signal penetrates through the entire 16 cm snow cover to be absorbed in the upper layer of sea ice. The location of $S_{H(-1\sigma)}$ is close to the location of the 50% TFMRA-assumed main scattering horizon, which is assumed to be at the snow/sea ice interface (Ricker et al., 2014). Therefore, existing 50% TFMRA retrievals are likely most applicable to brackish sea ice areas such as the Baltic Sea or the colder conditions of midwinter. In the case of snow

covers that are highly brine-wetted (i.e., $\varphi_{bs(+1\sigma)}$), the $S_{H(+1\sigma)}$ and δ_p are 3 cm and 4 cm below the air/snow interface, respectively (Figure 3). The $\Delta_{S(+1SE)}$ is thus 13 cm above the snow/sea ice interface.

3.3. First-Year Sea Ice Thickness Retrieval Correction and Error Analysis

Figure 4 illustrates the relative error (E_R) (%) for CS-2 monthly mean FYI thickness retrievals over the entire Arctic, for March 2016. It includes the original FYI retrievals ($T_{FYI(ORIG)}$) (Ricker et al., 2017) and the snow salinity-corrected T_{FYI} using Δ_S , $\Delta_{S(-1SE)}$, and $\Delta_{S(+1SE)}$ for the 16 cm snow pit case study data (equations (7) to (9)). Comparing first the running median and running mean lines for $T_{FYI(ORIG)}$ (bold versus dotted black lines in Figure 4), we note that at a FYI thickness of 1 m, the running median reduces E_R by 8.8% in relation to the running mean, and at 0.8 m, E_R is reduced by 23.6%.

Next, comparing the $T_{FYI(ORIG)}$ E_R running median with the SMOS E_R running median (black versus white lines in Figure 4), we note the difference in retrieval estimates between these two sensors. Adopting a 30% E_R threshold to define the FYI thickness regimes for which retrieval error is relatively high, it can be observed that the CS-2 $T_{FYI(ORIG)}$ E_R is high for FYI thicknesses <0.95 m, whereas SMOS E_R is high for FYI thicknesses >0.35 m. A SMOS-to-CS-2 uncertainty gap therefore exists between 0.35 m and 0.95 m, where confidence in FYI thickness estimates is limited.

To assess the reduction in E_R using the Δ_S correction, we compare the $T_{FYI(ORIG)}$ and $T_{FYI(\Delta_S)}$ running median values. At 1.6 m, the

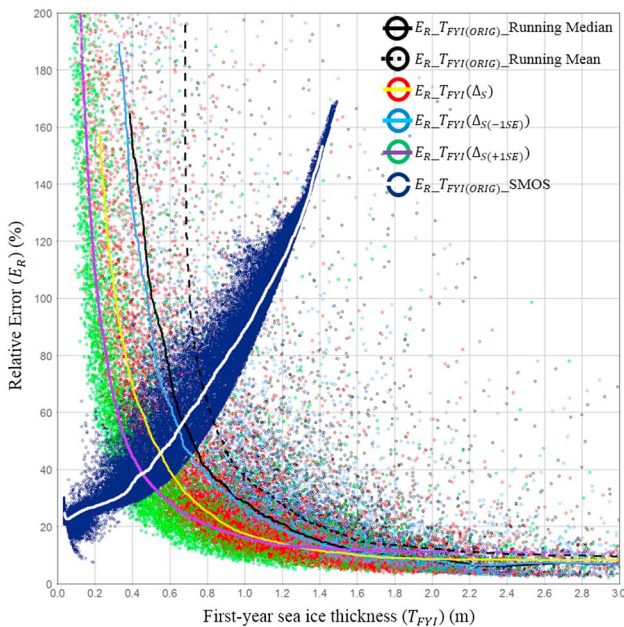


Figure 4. Relative error (E_R) for original CS-2 FYI thickness $T_{FYI(ORIG)}$ using the TFMRA50% retracker algorithm and SMOS, for March 2016. The yellow, blue, and purple lines represent the E_R for corrected CS-2 Arctic FYI thickness $T_{FYI(\Delta_S)}$, $T_{FYI(\Delta_{S(-1SE)})}$, and $T_{FYI(\Delta_{S(+1SE)})}$, respectively. The solid lines represent running medians. The bold black line and dashed black line represent the running median and running mean of E_R characteristic of $T_{FYI(ORIG)}$ following Ricker et al. (2017).

differences in E_R are negligible with all $E_R \approx 10\%$. However, as FYI thickness decreases, $T_{FYI}(\Delta_S)$ exhibits substantially reduced error. While the $T_{FYI(ORIG)}$ reaches $E_R \approx 30\%$ at 0.95 m, $T_{FYI}(\Delta_S)$ is 18.7% (yellow line in Figure 4), a reduction in E_R of 10.8%. $T_{FYI}(\Delta_S)$ does not reach 30% until 0.7 m, by which point the $T_{FYI(ORIG)}$ is 55%. Therefore, using our 30% E_R reference threshold, employing $T_{FYI}(\Delta_S)$ reduces the SMOS-to-CS-2 uncertainty gap for thin ice types by 0.25 m (from 0.35–0.95 m to 0.35–0.7 m).

All of the CS-2 running medians illustrate rapid increase in E_R at some inflection points as FYI thickness decreases. To define these inflection points, we identify the point on each curve where it reaches a slope of 100% per meter. For $T_{FYI(ORIG)}$, this inflection point occurs at around 0.95 m ice thickness, whereas the corrected $T_{FYI}(\Delta_S)$ does not exhibit such a steep increase until 0.65 m ice thickness (Figure 4).

The corrected T_{FYI} using $\Delta_{S(-1SE)}$ (hereafter $T_{FYI}(\Delta_{S(-1SE)})$) closely follows $T_{FYI(ORIG)}$ (blue line in Figure 4), which indicates that $T_{FYI}(\Delta_{S(-1SE)})$ aligns closely with the 50% threshold TFMRA and tracks close to the ice freeboard (Ricker et al., 2014), suggesting that the $T_{FYI(ORIG)}$ is more suitable for cold brine-free snow conditions on FYI.

The corrected T_{FYI} using the $\Delta_{S(+1SE)}$ (hereafter $T_{FYI}(\Delta_{S(+1SE)})$) (purple line in Figure 4) reduces E_R even more than using Δ_S . E_R of $T_{FYI}(\Delta_{S(+1SE)})$ is lower than that of $T_{FYI}(\Delta_S)$ by 4.6% at 0.8 m and by 9.7% at 0.6 m. However, $T_{FYI}(\Delta_{S(+1SE)})$ produces considerable overcorrection, due to a substantial number of negative freeboards, resulting in $T_{FYI(ORIG)} < 0$ m (Figure S3). Negative freeboard values are found in original F_I and corrected $F_I(\Delta_{S(+1SE)})$ estimates, $\sim 3.5\%$ and $\sim 28\%$, respectively (Figure S3). For $F_I(\Delta_S)$ estimates, $\sim 12\%$ are negative (not shown in Figure S3). Negative freeboards associated with the original F_I and $F_I(\Delta_S)$ estimates are likely the result of excess snow loading (via the modified Warren climatology) and/or inaccurate snow and ice densities. This effect is consistent with the ice freeboard estimates obtained using the TFMRA 80% retracker threshold, where the mean F_I was found to be negative during November 2013, and close to sea level in March 2013 (Ricker et al., 2014).

4. Conclusion

We have derived an estimate of the effect of snow salinity on CS-2-derived Arctic FYI freeboard and thickness estimates. A thickness-dependent snow salinity correction factor is added to the existing ice freeboard estimation method, based on a theoretically derived main radar scattering horizon at the CS-2 frequency of 13.575 GHz. We use in situ snow thermophysical property measurements, sampled from numerous undeformed and slightly deformed FYI locations within the Canadian Arctic during late winter season. Our simulations highlight the substantial effect that brine-wetted snow has on the main scattering horizon of CryoSat-2, which influences FYI freeboard and thickness estimates. Our corrected FYI thickness estimates using the snow salinity correction factor demonstrate reductions in CS-2 relative errors. The reductions are considerable at FYI thicknesses < 1 m. At 0.95 m, the relative error reduces by $\sim 11\%$ and at 0.7 m the error reduces by $\sim 25\%$. These reductions also help to close the uncertainty gap between SMOS and CS-2 thin ice thickness retrievals by 0.25 m. We find that current retrieval methods are likely more suited to very cold, low snow salinity FYI, which limits their scope. We also find that FYI with warm, highly saline snow has the potential to produce the highest retrieval errors. To increase confidence in CS-2 error analyses in all seasons, subsequent research should focus on using in situ FYI thickness data for validation, to quantify the error objectively. With the recent and rapid decline of MYI, and its replacement by FYI, the role of snow salinity should be considered whenever FYI freeboard is estimated using CryoSat-2 on local to pan-Arctic scales.

References

- Barber, D. G., & Hanesiak, J. M. (2004). Meteorological forcing of sea ice concentrations in the southern Beaufort Sea over the period 1979 to 2000. *Journal of Geophysical Research: Oceans*, 109, C06014. <https://doi.org/10.1029/2003JC002027>
- Barber, D. G., & Nghiem, S. V. (1999). The role of snow on thermal dependence of microwave backscatter over sea ice. *Journal of Geophysical Research*, 104, 25,789–25,803. <https://doi.org/10.1029/1999JC900181>
- Barber, D. G., Reddan, S. P., & LeDrew, E. F. (1995). Statistical characterization of the geophysical and electrical properties of snow on landfast first-year sea ice. *Journal of Geophysical Research*, 100, 2673–2686. <https://doi.org/10.1029/94JC02200>
- Cox, G. F., & Weeks, W. F. (1975). *Brine Drainage and Initial Salt Entrapment in Sodium Chloride Ice* (No. CRREL-RR-345). Hanover, NH: Cold Regions Research and Engineering Laboratory.
- Crocker, G. (1992). Observations of the snow cover on sea ice in the Gulf of Bothnia. *International Journal of Remote Sensing*, 3(13), 2433–2445.
- Davis, C. (1997). A robust threshold re-tracking algorithm for measuring ice-sheet surface elevation change from satellite radar altimeters. *IEEE Transactions on Geoscience and Remote Sensing*, 35, 974–979.

Acknowledgments

The authors thank Mark Fuller and Patrick Duke of the University of Calgary for assistance with snow thickness and geophysical property data collection; David Roberts for assisting with graphical data representation; Natural Sciences and Engineering Research Council of Canada (NSERC) Discovery and Tools and Infrastructure grants to John Yackel, Randall Scharien, and Brent Else; Polar Continental Shelf Project (PCSP); and the Northern Scientific Training Program (NSTP) for financial and logistic support. The Centre for Earth Observation Science, University of Manitoba (principal investigator David Barber) is acknowledged for financial and logistical support for collection of field data. POLAR Knowledge Canada, Cambridge Bay (Dwayne Beattie and Angulalik Pedersen) is also acknowledged for logistical support for field data collection. The authors sincerely thank the three anonymous reviewers and the Editor for providing valuable suggestions to improve this paper. Processing of the CryoSat-2 sea ice thickness is funded by the German Ministry of Economic Affairs and Energy (Grant: 50EE1008), and data from March 2016 are obtained from <http://www.meereisportal.de> (Grant: REKLIM-2013-04). Processing of the SMOS data sea ice thickness was funded by EU project SIDARUS, and data from March 2016 are obtained from <http://www.meereisportal.de> (grant: REKLIM-2013-04).

- Denoth, A. (1989). Snow dielectric measurements. *Advances in Space Research*, 9(1), 233–243.
- Drinkwater, M. R., & Crocker, G. B. (1988). Modeling changes in the dielectric and scattering properties of young snow covered sea ice at GHz frequencies. *Journal of Glaciology*, 34(118), 274–282.
- Drobot, S. D., & Barber, D. G. (1998). Towards development of a snow water equivalence (SWE) algorithm using microwave radiometry over snow covered first-year sea ice. *Photogrammetric Engineering and Remote Sensing*, 64(5), 415–423.
- Eastwood, S. (2012). OSI SAF sea ice product manual, v3. EUMETSAT. Satellite Application Facility on Ocean and Sea Ice. Retrieved from <http://osisaf.met.no/p/ice/>
- Frankenstein, G., & Garner, R. (1967). Short note: Equations for determining the brine volume of sea ice from -0.5° to -22.9°C . *Journal of Glaciology*, 6(48), 943–944.
- Fuller, M. C., Geldsetzer, T., Gill, J. P., Yackel, J. J., & Derksen, C. (2014). C-band backscatter from a complexly-layered snow cover on first-year sea ice. *Hydrological Processes*, 28(16), 4614–4625.
- Geldsetzer, T., Langlois, A., & Yackel, J. J. (2009). Dielectric properties of brine-wetted snow on first-year sea ice. *Cold Regions Science and Technology*, 58, 47–56.
- Grosfeld, K., Treffeisen, R., Asseng, J., Bartsch, A., Bräuer, B., Fritsch, B., ... Weigelt, M. (2016). Online sea-ice knowledge and data platform <www.meereisportal.de>. Polarforschung, Bremerhaven. Alfred Wegener Institute for Polar and Marine Research & German Society of Polar Research, 85(2), 143–155.
- Hendricks, S., Ricker, R., & Helm, V. (2016). *AWI CryoSat-2 Sea Ice Thickness Data Product, Data product manual*. Bremerhaven, Germany: Alfred-Wegener-Institut.
- Iacozza, J., & Barber, D. G. (1999). An examination of the distribution of snow on sea-ice. *Atmosphere-Ocean*, 37(1), 21–51.
- Kaleschke, L., Tian-Kunze, X., Maaß, N., Ricker, R., Hendricks, S., & Drusch, M. (2015). Improved retrieval of sea ice thickness from SMOS and Cryosat-2. In *2015 IEEE International Geoscience and Remote Sensing Symposium (IGARSS)* (pp. 5232–5235). Milan, Italy: IEEE.
- Kern, S., Khvorostovsky, K., Skourup, H., Rinne, E., Parsakhoo, Z. S., Djepa, V., ... Sandven, S. (2015). The impact of snow depth, snow density and ice density on sea ice thickness retrieval from satellite radar altimetry: Results from the ESA-CCI Sea Ice ECV Project Round Robin Exercise. *The Cryosphere*, 9(1), 37–52.
- King, J., Howell, S., Derksen, C., Rutter, N., Toose, P., Beckers, J. F., ... Richter-Menge, J. (2015). Evaluation of Operation IceBridge quick-look snow depth estimates on sea ice. *Geophysical Research Letters*, 42, 9302–9310. <https://doi.org/10.1002/2015GL066389>
- Kurtz, N. T., & Farrell, S. L. (2011). Large-scale surveys of snow depth on Arctic sea ice from Operation IceBridge. *Geophysical Research Letters*, 38, L20505. <https://doi.org/10.1029/2011GL049216>
- Kwok, R. (2014). Simulated effects of a snow layer on retrieval of CryoSat-2 sea ice freeboard. *Geophysical Research Letters*, 41, 5014–5020. <https://doi.org/10.1002/2014GL060993>
- Kwok, R., & Cunningham, G. F. (2015). Variability of Arctic sea ice thickness and volume from CryoSat-2. *Philosophical Transactions of the Royal Society A*, 373(2045), 20140157.
- Laxon, S. W., Giles, K. A., Ridout, A. L., Wingham, D. J., Willatt, R., Cullen, R., ... Hendricks, S. (2013). CryoSat-2 estimates of Arctic sea ice thickness and volume. *Geophysical Research Letters*, 40, 732–737. <https://doi.org/10.1002/grl.50193>
- Lorrain, P., Corson, D. R., & Lorrain, F. (1988). *Electromagnetic Fields and Waves*, (Third ed. p. 754). New York: W.H. Freeman & Company.
- Maslanik, J., Stroeve, J., Fowler, C., & Emery, W. (2011). Distribution and trends in Arctic sea ice age through spring 2011. *Geophysical Research Letters*, 38, L13502. <https://doi.org/10.1029/2011GL047735>
- Nandan, V., Geldsetzer, T., Islam, T., Yackel, J. J., Gill, J. P., Fuller, M. C., ... Duguay, C. (2016). Ku-, X- and C-band measured and modeled microwave backscatter from a highly saline snow cover on first-year sea ice. *Remote Sensing of Environment*, 187, 62–75.
- Nandan, V., Scharien, R., Geldsetzer, T., Mahmud, M., Yackel, J. J., Islam, T., ... Duguay, C. (2017). Geophysical and atmospheric controls on Ku-, X- and C-band backscatter evolution from a saline snow cover on first-year sea ice from late-winter to pre-early melt. *Remote Sensing of Environment*, 198, 425–441.
- Ricker, R., Hendricks, S., Helm, V., Skourup, H., & Davidson, M. (2014). Sensitivity of CryoSat-2 Arctic sea-ice freeboard and thickness on radar-waveform interpretation. *The Cryosphere*, 8(4), 1607–1622.
- Ricker, R., Hendricks, S., Kaleschke, L., Tian-Kunze, X., King, J., & Haas, C. (2017). A weekly arctic sea-ice thickness data record from merged CryoSat-2 and SMOS satellite data. *The Cryosphere*, 11(4), 1607–1623.
- Ricker, R., Hendricks, S., Perovich, D. K., Helm, V., & Gerdes, R. (2015). Impact of snow accumulation on CryoSat-2 range retrievals over Arctic sea ice: An observational approach with buoy data. *Geophysical Research Letters*, 42, 4447–4455. <https://doi.org/10.1002/2015GL064081>
- Stogryn, A., & Desargant, G. (1985). The dielectric properties of brine in sea ice at microwave frequencies. *IEEE Transactions on Antennas and Propagation*, 33(5), 523–532.
- Tian-Kunze, X., Kaleschke, L., Maaß, N., Mäkynen, M., Serra, N., Drusch, M., & Krumpfen, T. (2014). SMOS-derived thin sea ice thickness: Algorithm baseline, product specifications and initial verification. *The Cryosphere*, 8(3), 997–1018.
- Tilling, R. L., Ridout, A., Shepherd, A., & Wingham, D. J. (2015). Increased Arctic sea ice volume after anomalously low melting in 2013. *Nature Geoscience*, 8(8), 643–646.
- Ulaby, F. T., Stiles, H. W., & Abdelrazik, M. (1984). Snowcover influence on backscattering from terrain. *IEEE Transactions on Geoscience and Remote Sensing*, GE-22(2), 126–133.
- Warren, S. G., Rigor, I. G., Untersteiner, N., Radionov, V. F., Bryazgin, N. N., Aleksandrov, Y. I., & Colony, R. (1999). Snow depth on Arctic sea ice. *Journal of Climate*, 12(6), 1814–1829.
- Webster, M. A., Rigor, I. G., Nghiem, S. V., Kurtz, N. T., Farrell, S. L., Perovich, D. K., & Sturm, M. (2014). Interdecadal changes in snow depth on Arctic sea ice. *Journal of Geophysical Research: Oceans*, 119, 5395–5406. <https://doi.org/10.1002/2014JC009985>
- Willatt, R., Laxon, S., Giles, K., Cullen, R., Haas, C., & Helm, V. (2011). Ku-band radar penetration into snow cover on Arctic sea ice using airborne data. *Annals of Glaciology*, 52(57), 197–205.
- Winebrenner, D. P., Bredow, J., Fung, A. K., Drinkwater, M. R., Nghiem, S., Gow, A. J., ... West, R. D. (1992). Microwave sea ice signature modeling. In F. Carsey (Ed.), *Microwave Remote Sensing of Sea Ice* (pp. 137–175). Washington, DC: American Geophysical Union.
- Zheng, J., Geldsetzer, T., & Yackel, J. (2017). Snow thickness estimation on first-year sea ice using microwave and optical remote sensing with melt modelling. *Remote Sensing of Environment*, 199, 321–332.